Journal of Applied Polymer Science

Role of nanoclay distribution on morphology and mechanical behavior of rubber-modified polyolefins

Moein Babaienejad, Reza Bagheri
Department of Materials Science and Engineering, Sharif University of Technology, Tehran, Iran, 11155-9466
Correspondence to: R. Bagheri (E-mail: rezabagh@sharif.edu)

ABSTRACT: Polyolefin blends have attracted great attention for years because of their improved physical and mechanical properties; especially when micro/nanofillers are present in the compound. Previous investigations have proven that incorporation of small amounts of nanoclay can enhance physical and mechanical properties of the polymer. This research has focused on the role of clay distribution on morphology and mechanical properties of ternary nanocomposites containing a rubbery phase. High-density polyethylene/ethylene vinyl acetate/clay (HDPE/EVA/clay) is opted as a typical model for this purpose. EVA is selected to act as both compatibilizer, because of having polar vinyl groups, and rubber-modifier, because of its elastomeric properties, in this ternary blend. Nanocomposite preparation was performed via one- and two-step mixing routes to achieve two different desired morphologies. Tensile and Izod impact tests, and different microscopic techniques, were used to evaluate nanostructure and mechanical performance of blends. Results of the study proved two distinct morphologies forming as a result of different incorporated processing techniques. Mixing components simultaneously leaded to a structure in which, clay platelets are located at the HDPE/EVA interface, whereas in the two-step processing route, most of the clay platelets are encapsulated by the EVA second phase particles. According to the results of the current study, encapsulation of the nanofillers by the second rubbery phase harms mechanical properties of the blend and should be avoided. On the other hand, much better mechanical performance is obtained when the clay platelets are located at the matrix/rubber interface. © 2015 Wiley Periodicals, Inc. J. Appl. Polym. Sci. **2015**, *132*, 41993.

KEYWORDS: clay; mechanical properties; morphology; polyolefins

Received 26 August 2014; accepted 12 January 2015
DOI: 10.1002/app.41993

INTRODUCTION

As a novel kind of composites, Polymer/Layered Silicate (PLS) nanocomposites have been a matter of interest for researchers over the past decade. The presence of small amounts of layered silicates in the composite leads to considerable improvements in the mechanical properties, gas permeability, thermal stability and other physicochemical properties, in comparison to virgin polymer.[1–4] Depending on the nature of the components used (layered silicate, organic cation, and polymer matrix) and the method of preparation, three main types of composites may be obtained when a layered clay is associated with a polymer: phase-separated microcomposite, intercalated, and exfoliated.[1] In exfoliated PLS nanocomposites, extensive polymer penetration into galleries generates a structure, in which individual nanometer-thick silicate layers of organoclays, are uniformly dispersed in the polymer matrix. In intercalated PLS nanocomposites, on the other hand, the multilayer structure of the silicates is retained, with alternating polymer/silicate layers and a repeat spacing lager than that of the organoclay. Significant property enhancements are often observed for exfoliated PLS nanocomposites[5,6] because of more matrix/filler interaction, which is the consequence of larger surface area per unit volume.[7]

Although many pristine polymers have been used to prepare nanocomposites with layered silicate, considerable interest in polyolefin/clay nanocomposites has emerged because of their potential to offer enhanced performance in many engineering applications, such as packaging, automobile, etc. Especially, polypropylene (PP) and polyethylene (PE) are widely used in packaging, consumer goods, pipes, cable insulation, etc.[7] Because of the hydrophobic character of polyolefins, interaction of hydrophilic clay and matrix is not sufficient to attain an exfoliated or intercalated structure.[8,9] To overcome problems associated with poor phase adhesion in polyolefin/clay systems a compatibilizer needs to be used.[10] This compatibilizer usually is a copolymer with a nonpolar backbone and a grafted polar monomer, for example, like the standard polyethylene or polypropylene grafted with maleic anhydride (PEgMA or PPgMA, respectively) or polyethylene grafted with acrylic acid (PEgAA).[11] Another copolymer, ethylene–vinyl acetate (EVA) can also be used as compatibilizer. Studies have shown that the

addition of EVA in nanocomposites of low-density polyethylene (LDPE) and high-density polyethylene (HDPE) with organoclays improved the polymer intercalation into the clay's platelets.[12]

On the other hand, most popular polyolefins like HDPE and PP are brittle at high strain rates and low temperatures, that makes their application limited in some industrial sectors.[13] Although addition of clay to polymers generally causes enhanced tensile stiffness and strength, just under certain circumstances does it lead to toughness increase.[14,15] To prepare tougher materials, elastomer particle addition is needed to restore the tensile ductility and impact toughness of polymer–clay nanocomposites.[14] Recently, this approach for polymer modification has been used to combine polymer blends and nanocomposites properties, resulting in high impact strength and modulus at the same time.[16] For this purpose, incorporation of elastomers like EPR, EPDM, SBS, and EVA into polyolefins matrix is prevalent.[4,17] Enhancement extent depends on different parameters such as size, shape, homogeneity of second phase and filler and generally, it can be said that nanocomposite microstructure plays a pivotal role.[18]

The presence of organoclay in a rubber-modified polyolefin can vary rheological parameters of the ternary system during melt processing, which leads to morphological differences, in comparison to virgin blend. In addition, the location of clay platelets in the blend affects on final morphology and mechanical properties of nanocomposites. The latter has recently attracted researchers' attention. Generally speaking, the localization of nanoparticles like organoclay, as well as other morphological features of polymer blends is governed by thermodynamics and/or kinetic effects. The main discussed thermodynamically controlling parameter of the localization is the wetting parameter ω_{AB}. However, because of the viscosity of the system, the equilibrium dictated by ω_{AB} may never be reached. Hence, concerning the kinetic effects, the final localization of fillers in a polymer pair is guided by the sequence of mixing of the components, the viscosity ratio, the composition, the temperature, the shear rate, and the time of mixing.[19] Few publications have studied the relationship between the location of the organoclay in blends with elastomeric dispersed particles and the corresponding morphology and mechanical properties.[19] For instance, it has been proven that in PBT/EVA-g-MA/organoclay[6] and Nylon 66/SEBS-g-MA/organoclay[18,20] systems, higher stiffness and lower toughness, as the consequence of the addition of organoclay occurs when the organoclay platelets are located in the continuous phase, not in the aggregated phase. On the other hand, Lee *et al.*,[21] found that the addition of organoclay to PP/ethylene–octene elastomer blend can lead to an increase in the toughness relative to the neat blend. These authors believe that organoclay is in the continuous phase and the subsequent decrease in the size of the dispersed elastomeric phase improves the toughness and compensates at least intrinsic decrease of the toughness by the introduction of the rigid organoclay phase. Kelnar *et al.*[22,23] found that in polyamide-6/EPR/organoclay ternary blends, toughness is more than virgin blend, when stacks of the clay are located around the EPR disperse particles but not in the matrix. As Li *et al.*[24] claim, in the ternary blend of PP/SBS/organoclay, the clay platelets were located in the dispersed SBS phase and the toughness increased with the addition of organoclay to the blend. Martins *et al.*[16] examined two kinds of organoclays in PP/EVA/organoclay system and insisted on the role of organoclay type on morphology and mechanical properties. They reported that when the organoclay was in the dispersed EVA phase, the particles of this phase had a lamellar shape, and the impact strength was considerably higher than for the neat blend. On the other hand, for the ternary nanocomposites where the platelets were not well dispersed in the EVA phase, the impact strength was decreased relative to the neat blend. Despite all these, an in-depth understanding of the relationship between the location of clay and its corresponding final morphology and mechanical properties of nanocomposites, is still lacking.

In this work, we tried to achieve two desired morphologies in a model system, HDPE/EVA/organoclay, and then to precisely define how clay location affects morphology and mechanical properties. The stimulus for using HDPE as the matrix in this ternary system is its good processability, low cost, and wide range of applications in the industry. We used ethylene vinyl acetate (EVA) as the rubber-modifier. EVA is a random copolymer with polar groups which makes a two phase rubber-modified structure in HDPE matrix and also enhances polarity of the polymer and thus, facilitates clay dispersion in the matrix. Meanwhile, it is expected that clay platelets tend to go toward EVA because of the polarity differences with HDPE matrix resulting in clay reach EVA domains. Our former investigations show that it is feasible to have samples with the same compositions, and different microstructures in terms of location of clay platelets, by changing blending sequence. Earlier studies in our research group have also shown that at EVA/clay ratio of 4 : 1, the compatibilizing effect of EVA is enough to have identical dispersion of clay platelets, regardless of the compounding procedure. Therefore, we used this technique to prepare nanocomposites with a major distinction; that is, the location of clay in the microstructure.

EXPERIMENTAL

Materials

HDPE BL3 (MFI = 1.2 g/10 min; 190°C, 5 kg) from Shazand (Arak) Petrochemical Corporation, Iran, and EVA Escorene Ultra FL 02020 (MFI = 20 g/10 min; 190°C, 2.160 kg, vinyl acetate content = 20 wt %) from Exxonmobil Chemical Company, China, organoclay DK1 from Fenghong Clay Chemical Company, China, were used as received. Sample preparation for clay-containing ones was done by two ways:

1. Compounding Clay and EVA, where the EVA/Clay ratio was 4 and then mixing provided master-batch with HDPE.
2. Compounding clay, EVA, and HDPE simultaneously.

Our rationale to use one- and two-step mixing process was to deliberately change the location of clay in the mixture.

All materials were dried for at least 12 h at 60°C before melt processing. Melt mixing was performed by a contour-rotating twin screw extruder ($L = 1.2$ m, $D = 53$ mm) in a successive

Table I. Sample's Compositions and Symbols in This Article

Symbol	Process	Composition		
		HDPE	EVA	CLAY
HDPE	—	100	0	0
HDEV	1-Step Mixing	90	10	0
S2	2-Step Mixing	87.5	10	2.5
S1	1-Step Mixing	87.5	10	2.5

temperature range of 160–180°C. Testing specimens, including tensile and Izod impact bars, were injection molded, whereas the barrel temperature profile of the injection molding apparatus was set between 170 and 185°C from feed zone to nozzle. The mold temperature was held at about 60°C. Table I shows samples and their symbols used in this article.

Tensile Test

The modulus of elasticity and yield stress of pure HDPE, HDEV, and the nanocomposites were measured according to ASTM D638. The tests were performed on a universal Hounsfield frame (H10KS) at 5 mm/min crosshead speed. A 100SC extensometer was incorporated to determine the modulus of elasticity. Each data reported is the average of at least 10 measurement records.

Impact Test

Rectangular bars of 127 × 12.8 × 6.34 (mm) were used for Izod impact tests. The specimens were tested using a 5-J hammer (from Santam Co.) according to ASTM D256-88. Five measurements were done for every data recording.

Differential Scanning Calorimetry

The crystallization behavior of pure high-density polyethylene and HDPE/EVA/Clay nanocomposites were studied using a TA Instrument (Q100) differential scanning calorimeter (DSC). About 5 mg of each sample was heated up from 25 to 170°C at a heating rate of 10°C/min in an aluminum pan. The sample was then held for 2 min at 170°C to eliminate thermal history of the sample, induced during the injection molding process, before being cooled to room temperature. Crystallization peak in the cooling cycle was used to measure crystallization rate,[25] which reveals heterogeneous nucleation rate for clay containing samples.

Wide Angle X-ray Diffraction

Investigation of clay dispersion and dimension assessment of HDPE crystallites was performed by a STOE diffractometer on milled Izod bars. An acceleration voltage of 40 kV and a current of 40 mA were applied using Cu-Kα radiation. The crystal thickness perpendicular to the reflection plane, l, was calculated using Scherrer's equation:

$$l = \frac{K\lambda}{\beta_0 \cos\theta}$$

$$\beta_0^2 = \beta_M^2 - \beta_I^2$$

where $ß_0$ is the width of the diffraction beam (rad); $ß_M$ is the measured width of the diffraction beam (rad); $ß_I$ is the instrumental broadening (rad); K is the shape factor of crystalline thickness, related to $ß_0$ and l. When $ß_0$ is defined as the half-height width of the diffraction peak, $K = 0.9$.[26]

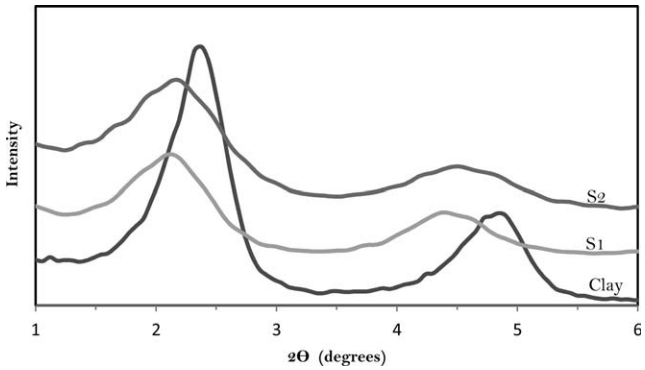

Figure 1. WAXD scans for neat organoclays, S1, and S2 nanocomposites.

Scanning Electron Microscopy

Cryofractured surface of notched Izod impact specimens (cross section) at room temperature was studied using scanning electron microscopy (SEM; VEGA/TESCAN) after coating with gold to minimize electrostatic charging. The cryofractured surface morphology of two ternary nanocomposites was observed using an electron accelerating voltage of 10 kV.

Transmission Electron Microscopy

To examine the dispersion of clay tactoids and their location in the matrix, transmission electron microscopy (TEM) was used. Ultra-thin sections with ~70 nm thickness were cut from the injection-molded Izod samples. Ultramicrotomy was conducted using a Reichert-Jung Ultracut-EVVR equipped with a diamond knife. For staining, ultrathin sections on 300 mesh copper grid were exposed to osmium tetraoxide (OsO4) vapor for about 1 day. During the staining procedure, the EVA phase became darker than the HDPE phase, and thus, it was possible to determine location of organoclay platelets or tactoids. TEM observation was performed on a Zeiss - EM10C TEM, operated at 80 kV.

Transmission Optical Microscopy

To observe the damage zone in front of crack tip, single edge notched three-point bending (SEN-3PB) tests were performed according to ASTM D5045. Pre-cracks were produced by means of a razor blade, which had been previously chilled at low temperature. This test was performed using a universal Hounsfield frame (H10KS) at a cross-head speed of 1 mm/min. After some deformation occurred, for observation of the deformation mechanism, the lateral surfaces were polished from both sides to reach a thickness of approximately < 100 μm in the middle of the samples. The thin sample, containing the damage zone was studied by Olympus EMP3 optical microscope under white light (Bright Field).

RESULTS AND DISCUSSION

Morphology

WAXD. XRD results on S1 and S2 prove the formed structures to be intercalated. As observed in Figure 1, peaks referring to

Table II. Organoclay Interlayer Spacing Obtained by WAXD

	2θ	d_{001} (°A)
Neat Organoclay	2.45	36.03
S1	2.09	42.2
S2	2.14	41.3

(100) basal planes in S1 and S2 nanocomposites, have a left shift compared with pristine clay which is due to the placement of polymer chains between clay layers and enlargement of the inter-plane distance. Table II shows dispersion of nanoclay in S1 and S2 to be almost the same. Thus, the dispersion of nanoclay can not have a sizeable role in mechanical properties of the two nanocomposites and variations in properties should be completely addressed to differences in morphologies.

SEM. SEM photomicrographs of cryofractured surfaces of S1 and S2 ternary nanocomposites are depicted in Figure 2. Comparison of these two morphologies of the ternary nanocomposites of HDPE/EVA/Clay, qualitatively reveals that in S1 nanocomposite the shape of the EVA particles is irregular, with smaller curvature and larger anisotropy than the particles in S2 sample. In S2, EVA/Clay masterbatch is mixed with HDPE during blending process, so elastomer phase has maximum viscosity in comparison to HDPE. Consequently, EVA/clay domains are coarser. Mixing three components (HDPE, EVA, and Clay) simultaneously, on the other hand, leads to a less viscous second phase and a more viscous HDPE in comparison to two-step mixing process; so finer elastomer particles with wider size distribution are achieved.

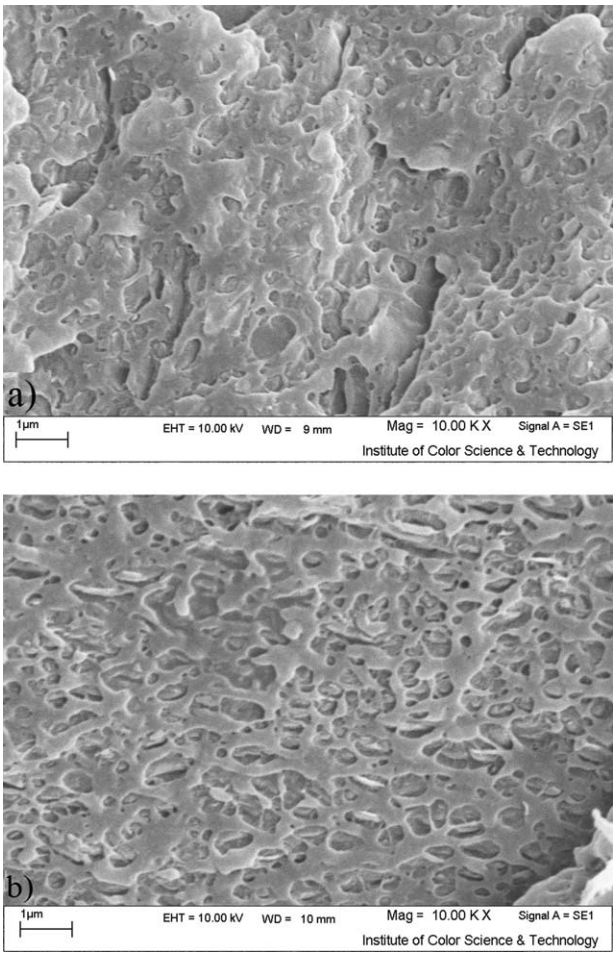

Figure 2. SEM micrographs of cryofractured surfaces for: (a) S1 and (b) S2 nanocomposites.

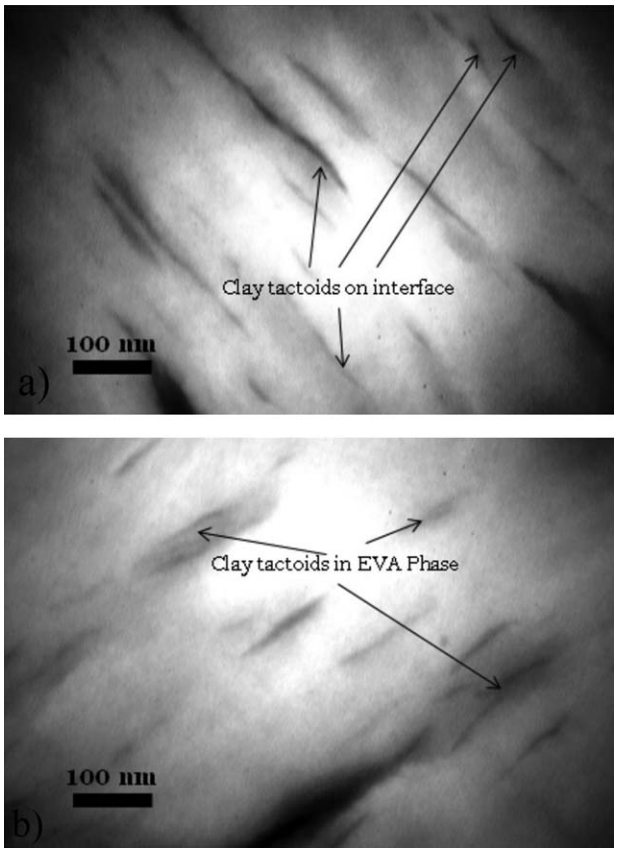

Figure 3. TEM micrographs of HDPE/EVA/Organoclay ternary nanocomposites: (a) and (b) micrographs with magnification of 31,500× of S1 and S2 mixtures, respectively.

TEM. Figure 3(a,b) shows TEM micrographs of S1 and S2 ternary nanocomposites. In both S1 and S2 nanocomposites, clay small and large tactoids are visible, and TEM micrographs do not show a significant number of individual clay platelets. As observed in these TEM images and verified by XRD results, the dominant structure is the intercalated structure. In the TEM micrographs, the difference between clay locations in these two morphologies is evident. Darker phase is EVA, as it is stained by OsO_4. EVA is more compatible than HDPE with clay tactoids—for having vinyl polar groups—and clay particles tend to reside in EVA phase. Because in the S2 nanocomposite, EVA/clay masterbatch has been added to HDPE, clay is included in the EVA phase from the beginning. Because of better compatibility and adhesion with EVA, diffusion of clay outward from this phase seems undesirable. Hence, the HDPE background is almost deplete from nanoclay. In S1 nanocomposite, in contrast, the existence of clay particles in HDPE background, HDPE/EVA interface and EVA is possible due to the simultaneous mixing of

Table III. HDPE Crystallite Size and Crystallization Rate for HDEV, S1, and S2 Samples

	XRD test Crystallite size (nm)	DSC test Crystallization rate (mW/°C)
HDEV	33	6.9
S1	29	11.5
S2	30	9.7

the three components. As mentioned earlier, the interaction between clay and EVA makes the nanoclay particles move toward EVA. During melt processing, nanoclay particles in HDPE background migrate toward the HDPE/EVA interface as their presence can be seen in Figure 3(a).

DSC and XRD. The role of nanoclay as a nucleation agent in intercalated and exfoliated structures has been analyzed in previous investigations. The addition of nanoclay, leads to a decrease in the thickness of crystal lamellas, increase in T_C and rate of crystallization.[10,27] Addition of EVA to HDPE, on the other hand, because of their attractive molecular interactions, leads to loss of the degree of crystallinity in HDPE.[28,29] Although DSC results show no meaningful change in T_C, changes in crystallization rates are remarkable (Table III). In a comparison among S1, S2, and HDEV, the role of clay in heterogeneous nucleation of HDPE is observed in terms of lowered HDPE crystallite sizes and increased crystallization rates (as compared with clay-free samples). Higher nucleation rates in S1 compared with S2 might largely be addressed due to higher contact between the clay layers and the HDPE background. As with the XRD and DSC results, it is assumed that in S2 clay is more in the EVA, whereas S1 is more in contact with HDPE. These results are in accordance with the acquired TEM images.

As confirmed by the DSC, XRD, SEM, and TEM results, Figure 4 gives a proper illustration of the morphologies in S1 and S2. These two morphologies, resulting from variations in blending sequence, have been previously reported on other nanocomposites.[30]

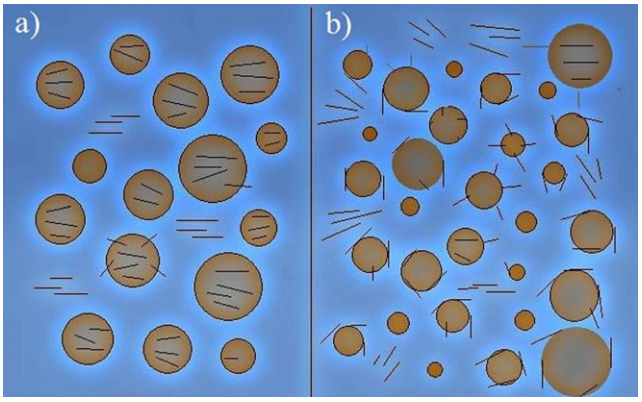

Figure 4. Morphology schematics for: (a) S2 and (b) S1 ternary nanocomposites. [Color figure can be viewed in the online issue, which is available at wileyonlinelibrary.com.]

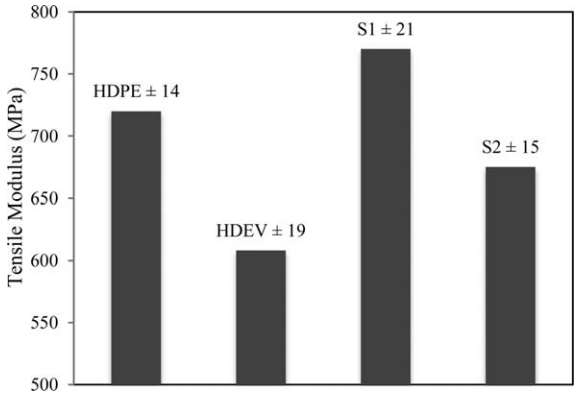

Figure 5. Comparative Tensile Modulus plot of HDPE, HDEV, S1, and S2 nanocomposites.

Mechanical Properties

Figures 5 and 6 show diagrams of tensile modulus, yield stress, and Izod impact strength for neat HDPE, HDEV, S1, and S2 nanocomposites. As with the measured values, S1 nanocomposite shows larger improvements compared with other samples. Previous studies have shown that elastic modulus of a nanocomposite depends on the modulus of its elements, whereas yield strength relies much more on particle–matrix adhesion.[31] This is why the yield strength improvement in S1 is better than S2, because of the role of EVA in S1 by improving adhesion between clay and HDPE. Meanwhile in S2, soft EVA surrounds clay and practically clay layers are not loaded that much. In terms of elastic modulus, the same comparison between S1 and S2 stays true. HDEV, in which 10% EVA is added to HDPE, has the lowest elastic modulus and yield stress because the elastomeric EVA phase is added to HDPE. Considering an elastic modulus of 35 MPa for pure EVA, Lever law calculations predicts a 670 MPa elastic modulus for HDEV, which is higher compared with the results of experiments. It can be due to crystalline changes in HDPE with the addition of EVA. Elastic modulus and yield stress for S2 lies between those of HDPE and HDEV. TEM images and the placement of clay particles properly explain these results, that is, the clay-containing second phase conserving its rubbery identity, is now stiffer.

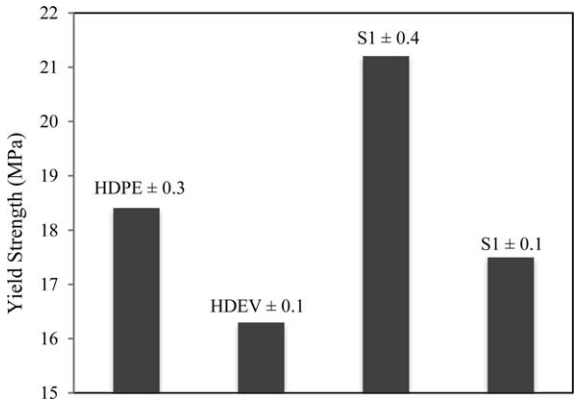

Figure 6. Comparative Yield strength plot of HDPE, HDEV, S1, and S2 nanocomposites.

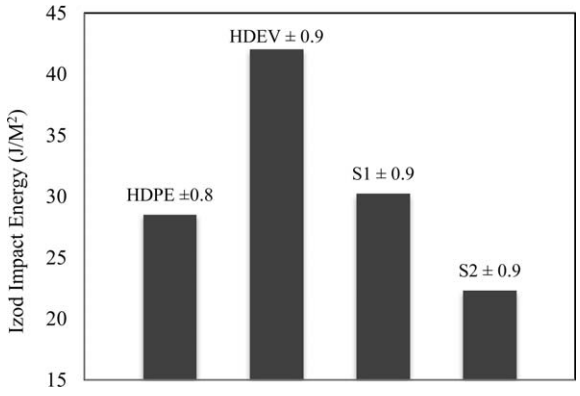

Figure 7. Comparative Izod Impact strength plot of HDPE, HDEV, S1, and S2 nanocomposites.

Figure 7 also presents the notched Izod impact strength of HDPE, HDEV, S1, and S2 samples. Incorporation of 10 wt % EVA into HDPE matrix makes it approximately 50% tougher. Dispersed rubber EVA particles enhance toughness via different mechanisms such as debonding, cavitation, and plastic deformation facilitation of the HDPE matrix.

A comparison between HDEV and S1 or S2 nanocomposites reveals that the addition of clay to the blend is detrimental in terms of toughness, whereas both improvement and deterioration of blend impact strength, by adding of clay has been reported in the literature.[16,18] Stress concentration in the vicinity of clay tactoids and the consequent crack initiation may be a rationale for depressed toughness. Clay tactoids can also enhance toughness via mechanisms like: debonding and delamination.[32] According to Izod impact values, S1 nanocomposite is tougher than S2, which can be illustrated by following reasons: (1) Finer elastomer particles with wider size distribution are formed in S1 nanocomposite, according to SEM micrographs, presented in Figure 2. This kind of morphology boosts plastic deformation in HDPE matrix and leads to higher toughness of nanocomposite. (2) Presence of clay in the EVA phase makes it stiffer and hinders elastomer cavitation, which is an active toughening mechanism, so that the toughening efficiency of the EVA is decreased. Dasari *et al.*[18] also reported deleterious effect of clay presence, either intercalated or exfoliated, in elastomer phase in Nylon 66/SEBS-g-MA/organoclay ternary nanocomposites. TOM micrographs of the tip of propagating crack are indicated in Figure 8 for HDPE, HDEV, S1, and S2 nanocomposites. Intense darkness, which is related to crazes and plastic deformation intensity, can be seen in front of the HDEV crack tip. There is an evident correlation between the intensity of plastic deformation zone and Izod impact strength quantities. HDEV is toughest according to both TOM micrographs and Izod impact strength results. It can be deducted from TOM micrographs, that S1 nanocomposite tends to have a fracture behavior like HDEV, but the presence of some stress concentrators around crack tip facilitate its propagation and results in a lower toughness than HDEV. Resemblance between TOM micrographs of S2 nanocomposite and neat HDPE may be enough to vote for inefficient role of elastomer phase, in case of toughness. Therefore, it can be concluded that, clay location plays a basic role in terms of affecting cavitation and matrix plastic deformation mechanisms.

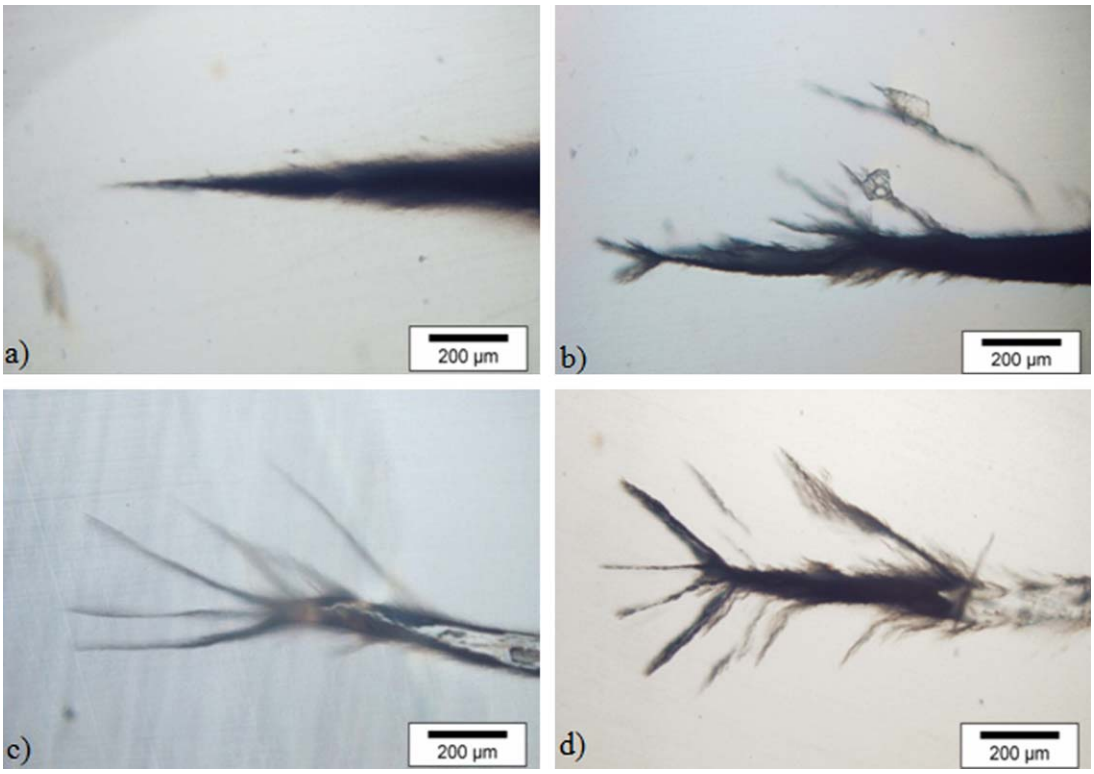

Figure 8. TOM micrographs presenting damage zone in front of crack tip at 10× magnification for: (a) HDEV, (b) S1, (c) HDPE, and (d) S2. [Color figure can be viewed in the online issue, which is available at wileyonlinelibrary.com.]

CONCLUSION

In this work, ternary nanocomposites of HDPE/EVA/organoclay with the weight ratios of 87.5/10/2.5, relatively, were prepared in two different blending sequences to achive different nanostructures. According to the results obtained, simultaneous blending of all constituents resulted in formation of a two-phase microstucture of EVA domains within the HDPE matrix, whereas intercalated clay platelets are mostly located around the HDPE/EVA. The alternative processing route consisted of making a masterbatch of EVA/nanoclay and then dilute it in the HDPE matrix. This two-step approach resulted again in a two-phase structure of EVA domains within the HDPE matrix; however, the intercalated clay platelets were resided mostly inside the EVA islands this time. According to the results, encapsulation of the nanofillers by the softer second rubbery phase was detrimental to tensile and impact properties of the blend. Transmission optical microscopy revealed that presence of the organoclay layers within the second rubbery phase reduces the ability of the EVA domains in localizing of plastic deformation in the matrix which negatively affects impact strength of the blend.

REFERENCES

1. Alexandre, M.; Dubois, P. *Mater. Sci. Eng. R Rep.* **2000**, *28*, 1.
2. Sinha Ray, S.; Okamoto, M. *Prog. Polym. Sci.* **2003**, *28*, 1539.
3. Srivastava, S.; Pramanik, M.; Acharya, H. *J. Polym. Sci. Part B: Polym. Phys.* **2006**, *44*, 471.
4. Kuila, T.; Srivastava, S. K.; Bhowmick, A. K.; Saxena, A. K. *Compos. Sci. Technol.* **2008**, *68*, 3234.
5. Zanetti, V. *Macromol. Mater. Eng.* **2000**, *1*, 2V9.
6. Li, X.; Park, H. M.; Lee, J. O.; Ha, C. S. *Polym. Eng. Sci.* **2002**, *42*, 2156.
7. Rezanavaz, R.; Razavi Aghjeh, M.; Babaluo, A. *Polym. Compos.* **2010**, *31*, 1028.
8. Wang, K. H.; Choi, M. H.; Koo, C. M.; Choi, Y. S.; Chung, I. *J. Polymer* **2001**, *42*, 9819.
9. Jeon, H.; Jung, H. -T.; Lee, S.; Hudson, S. *Polym. Bull.* **1998**, *41*, 107.
10. Gopakumar, T.; Lee, J.; Kontopoulou, M.; Parent, J. *Polymer* **2002**, *43*, 5483.
11. Teymouri, Y.; Nazockdast, H. *J. Mater. Sci.* **2011**, *46*, 6642.
12. Marini, J.; Branciforti, M. C.; Alves, R. M. V.; Bretas, R. E. S. *J. Appl. Polym. Sci.* **2010**, *118*, 3340.
13. Tanniru, M.; Yuan, Q.; Misra, R. D. K. *Polymer* **2006**, *47*, 2133.
14. Tjong, S.; Bao, S. *Compos. Sci. Technol.* **2007**, *67*, 314.
15. Kanny, K.; Jawahar, P.; Moodley, V. K. *J. Mater. Sci.* **2008**, *43*, 7230.
16. Martins, C. G.; Larocca, N. M.; Paul, D. R.; Pessan, L. A. *Polymer* **2009**, *50*, 1743.
17. Zebarjad, S. M.; Lazzeri, A.; Bagheri, R.; Seyed Reihani, S. M.; Frounchi, M. *Mater. Lett.* **2003**, *57*, 2733.
18. Dasari, A.; Yu, Z. -Z.; Mai, Y. -W. *Polymer* **2005**, *46*, 5986.
19. Taguet, A.; Cassagnau, P.; Lopez-Cuesta, J. M. *Prog. Polym. Sci.* **2014**, *39*, 1526.
20. Dasari, A.; Yu, Z. -Z.; Yang, M.; Zhang, Q. -X.; Xie, X. -L.; Mai, Y. -W. *Compos. Sci. Technol.* **2006**, *66*, 3097.
21. Lee, H. -S.; Fasulo, P. D.; Rodgers, W. R.; Paul, D. *Polymer* **2005**, *46*, 11673.
22. Kelnar, I.; Khunová, V.; Kotek, J.; Kaprálková, L. *Polymer* **2007**, *48*, 5332.
23. Kelnar, I.; Kotek, J.; Kaprálková, L.; Hromádková, J.; Kratochvil, J. *J. Appl. Polym. Sci.* **2006**, *100*, 1571.
24. Li, Y.; Wei, G. -X.; Sue, H. -J. *J. Mater. Sci.* **2002**, *37*, 2447.
25. Xu, W.; Ge, M.; He, P. *J. Polym. Sci. Part B: Polym. Phys.* **2002**, *40*, 408.
26. Wu, Q.; Lei, Y.; Yao, F.; Xu, Y.; Lian, K. 2007 First International Conference on Integration and Commercialization of Micro and Nanosystems, American Society of Mechanical Engineers, Sanya, Hainan, China, **2007**, pp 181.
27. Min, K. D.; Kim, M. Y.; Choi, K. -Y.; Lee, J. H.; Lee, S. -G. *Polym. Bull.* **2006**, *57*, 101.
28. Khonakdar, H.; Jafari, S.; Yavari, A.; Asadinezhad, A.; Wagenknecht, U. *Polym. Bull.* **2005**, *54*, 75.
29. Khonakdar, H. A.; Wagenknecht, U.; Jafari, S. H.; Hassler, R.; Eslami, H. *Adv. Polym. Technol.* **2004**, *23*, 307.
30. Zhang, M.; Lin, B.; Sundararaj, U. *J. Appl. Polym. Sci.* **2012**, *125*, E714.
31. Gloaguen, J.; Lefebvre, J. *Polymer* **2001**, *42*, 5841.
32. Cotterell, B.; Chia, J.; Hbaieb, K. *Eng. Fracture Mech.* **2007**, *74*, 1054.